BL3U

Exchange Interaction of the Rydberg Electron Bound by Doubly Charged Ions in Small Krypton Clusters Studied by Resonant Auger Spectroscopy

M. Nagasaka[1], T. Hatsui[2], H. Setoyama[1], N. Kosugi[1] and E. Rühl[3]

[1]*Institute for Molecular Science, Myodaiji, Okazaki 444-8585 Japan*
[2]*XFEL Project Head Office, RIKEN, Sayo-cho, Hyogo 679-5148, Japan*
[3]*Physikalische Chemie, Freie Universität Berlin, Takustr. 3, D-14195 Berlin, Germany*

In the core-to-Rydberg excitation of small krypton clusters, we have evaluated the surface-site dependent exchange (*EX*) interaction of the Rydberg electron with the nearest neighbor atoms by using X-ray absorption spectroscopy (XAS) [1 – 3]. After the resonant Auger decay following the core-to-Rydberg excitation, the spectator-type Auger final state can be regarded as a Rydberg electron bound by a doubly charged ion. The Rydberg electron bound by a singly charged core-hole state could be decreased by a doubly charged ion, increasing the short-range *EX* interaction. In the present work, we have evaluated the site-dependent *EX* energies of the Rydberg electron with the neighbor atoms in a doubly ion by using resonant Auger electron spectroscopy (RAS).

The experiments were performed at BL3U. Kr clusters with $\langle N \rangle \sim 15$ were formed by the supersonic gas expansion method. RAS spectra were measured with a hemispherical electron energy analyzer (SCIENTA SES-200 combined with MBS A-1).

Figure 1 shows RAS spectra after the Kr $3d_{5/2}^{-1}5p$ Rydberg excitation (91.37 eV) at the edge-site atom of small Kr clusters [1 – 3]. Because the ratio of edge and face sites is 3:1 in this excitation energy, the ratio in RAS is set to be 3:1 for the fitting procedure. As shown in Table 1 and Fig. 1, the observed final-state energies of both the 5p and 6p states are redshifted from the atomic one, indicating the induced polarization (*PL*) effect is dominant. As in the case of XAS, the energy shift of the Rydberg states ($i = 5, 6$) is given by $\Delta E_i(\text{RAS}) = PL\ (+2) + EX_i\ (+2)$, where $PL\ (+2)$ can be approximated as $4\ PL\ (+1)$. Table 1 shows *EX* in the doubly charged ion at different surface sites. *EX* (+2) is almost proportional to the number of nearest neighbor atoms within the first coordination shell. *EX* (+2) of the 5p state is 2.3 times larger than *EX* (+1) of the 5p state, indicating contraction of the Rydberg orbital as demonstrated in Fig. 2. Table 1 shows the 6p electron bound by the doubly charged ion has a similar *EX* energy to the 5p electron bound by the singly charged ion, also indicating contraction of the Rydberg orbital.

In conclusion, RAS spectra of small krypton clusters show redshifts from the atomic peaks, indicating the *PL* effect is dominant even in the lowest Rydberg state. Furthermore, the *EX* effect is also enhanced in the Auger final state, indicating the contraction of the Rydberg orbital under the stronger potential by the doubly charged ion. The *EX*

interaction of the Rydberg electron with the surrounding atoms is short-range interaction and is almost proportional to the number of the nearest neighbor atoms.
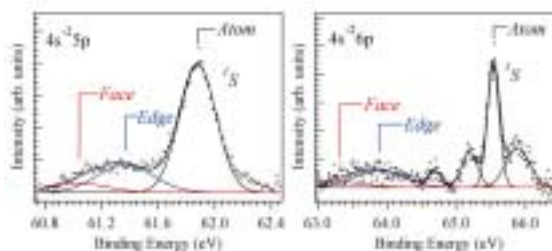

Fig. 1. RAS spectra of different surface sites in small krypton clusters for the $4s^{-2}5p$ and $4s^{-2}6p$ final states after the edge-site excitation in the $3d_{5/2}^{-1}5p$ state (91.37 eV).
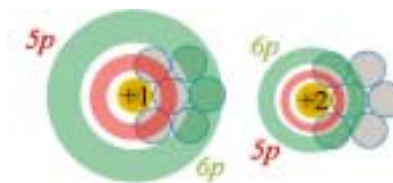

Fig. 2. Schematic Rydberg orbitals bound by singly and doubly charged ions at a surface site of small krypton clusters.

Table 1. Surface-site dependent *EX* energies (in eV) of the Rydberg electron bound by doubly charged ions of small krypton clusters. The bulk site corresponds to the large krypton clusters [4].

eV	ΔE	PL(+2)	EX (+2)	EX (+1)
4s⁻²5p				
Edge	-0.51	-2.28	1.77	0.74
Face	-0.84	-3.16	2.32	1.01
Bulk	-1.0	-4.3	3.3	1.47
4s⁻²6p				
Edge	-1.66	-2.28	0.62	0.22
Face	-2.22	-3.16	0.94	0.28
Bulk	-2.8	-4.3	1.5	0.42

[1] M. Nagasaka, T. Hatsui and N. Kosugi, in this volume.
[2] M. Nagasaka, T. Hatsui and N. Kosugi, J. Electron Spectrosc. Relat. Phenom. **166-167** (2008) 16.
[3] A. Knop, B. Wassermann and E. Rühl, Phys. Rev. Lett. **80** (1998) 2302.
[4] S. Peredkov *et al*., Phys. Rev. A **72** (2005) 021201.

Ⅲ-3. MOLECULAR SPECTROSCOPY AND DYNAMICS

Electron Ion Coincidence Spectroscopy of C_{60} Using Synchrotron Radiation Photoionization

C. Huang[1], H. Katayanagi[1, 2], B. P. Kafle[1], Md. S. I. Prodhan[2],
H. Yagi[1], K. Nakajima[1, 3] and K. Mitsuke[1, 2]

[1]Institute for Molecular Science, Okazaki 444-8585, Japan
[2]Graduate University for Advanced Studies, Okazaki 444-8585, Japan
[3]Science Research Center, Hosei University, Chiyoda-ku, Tokyo 102-8160, Japan

Photoelectron-photoion coincidence (PEPICO) spectroscopy is one of the most powerful methods for studying the kinetics and dynamics of chemical reactions involving excited molecules and ions. We therefore consider that unimolecular decomposition processes of fullerenes can be closely studied using a PEPICO method. This report presents a recent results obtained with an electron detector newly incorporated into a photoionization time-of-flight mass spectrometer using synchrotron radiation of $h\nu$ = 25-120 eV.

All experiments were carried out at the bending magnet beam line BL2B. Parent C_{60}^{z+} and fragment C_{60-2n}^{z+} ions ($n \geq 1$, z = 1-3) were measured at $h\nu$ = 50 – 120 eV. Since no small ionic carbon cluster C_m^{z+} (m = 1-5) was observed, the emission of neutral C_2 rather than C_m^{z+} is the main fragmentation channel of C_{60}^{z+}. As for the singly charged fragments, C_{58}^{+} and C_{56}^{+} were detected only at a very narrow $h\nu$ range. Above 60eV, their intensities become negligibly weak. This probably means that C_{60}^{+} ions with their internal energy higher than ~60 eV are stabilized rapidly by emitting one or two electron(s), *before* being converted to high-vibrationally excited states through nonadiabatic transitions (i.e. internal conversion) followed by statistical redistribution of excess energy and sequential ejection of C_2 units [2].

Taking mass spectra with scanning the monochromator allowed us to measure the ion yield curves for C_{60}^{z+} and C_{60-2n}^{z+} as a function of $h\nu$. The relative total photoionization cross section was calculated from the total ion yield curve of C_{60} and agrees well with our former results [1]. Next, the ratio $\sigma(C_{60-2n}^{z+})/\sigma(C_{60}^{+})$ between the relative photofragmentation cross section for C_{60-2n}^{z+} ($n \geq 1$, z = 1-3) and that for C_{60}^{+} was calculated from the yield curves of the respective ions. This ratio was measured also in pulsed ion sampling by applying a positive pulsed voltage to the repeller electrode. Figure 1 shows our results of $\sigma(C_{58}^{2+})/\sigma(C_{60}^{+})$ determined by PEPICO and pulsed ion sampling, together with the previous data of Reinköster *et al.* and Juranic *et al.* [3, 4]. The two data from the literature have been measured by pulsed ion sampling.

All the results of pulsed ion sampling show that the ratio almost levels off after passing its maximum value. In contrast, our PEPICO curve exhibits a pronounced decrease after the maximum at 75 eV. The ratios of $\sigma(C_{56}^{2+})/\sigma(C_{60}^{+})$ and $\sigma(C_{54}^{2+})/\sigma(C_{60}^{+})$

have similar tendencies. The different behaviors of the $\sigma(C_{60-2n}^{2+})/\sigma(C_{60}^{+})$ curves for different detection methods can be understood [2] from expectation that the magnitude of the average internal energy remaining in nascent C_{60}^{z+} ions produced in PEPICO is larger than that in pulsed ion sampling.

The appearance energies and peak positions of the yield curves for the fragment ions were found to be shifted in the higher $h\nu$ direction than those summarized in [2].
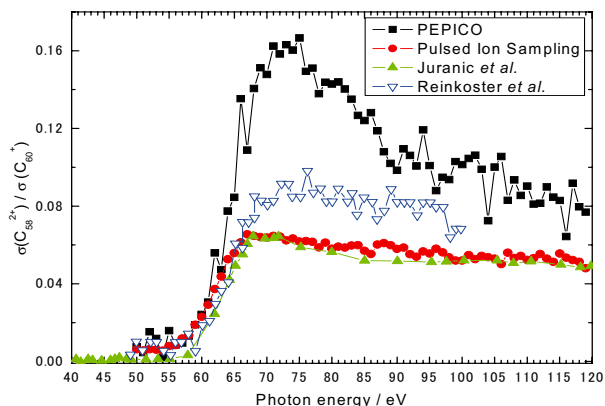

Fig. 1. Ratio between the photofragmentation cross section for C_{58}^{2+} and that for C_{60}^{+}.

[1] K. Mitsuke *et al.,* J. Phys. Chem. A **111** (2007) 8336.
[2] J. Kou *et al.,* Phys. Chem. Chem. Phys. **7** (2005) 119.
[3] B. Reinköster *et al.,* J. Phys. B **37** (2004) 2135.
[4] P. N. Juranic *et al.*, Phys. Rev. A **73** (2006) 042701.

III-3. MOLECULAR SPECTROSCOPY AND DYNAMICS

Performance of the Mass Gate Incorporated in the Photofragment Imaging Apparatus for Measuring Momentum Distributions in Dissociative Photoionization of Fullerenes

B. P. Kafle[1], H. Katayanagi[1, 2], C. Huang[1], S. I. Prodhan[2], H. Yagi[1] and K. Mitsuke[1, 2]

[1] *Institute for Molecular Science, Okazaki 444-8585, Japan*
[2] *Graduate University for Advanced Studies, Okazaki 444-8585, Japan*

We have developed a velocity imaging spectrometer, to obtain a reliable velocity distribution of the fullerene fragments using synchrotron radiation [1-3]. Uniqueness of this apparatus is incorporation of a cylindrical *mass gate* and *retarding grid* near the end of the drift tube which are used to eliminate the overlapping of images due to other ionic fragments. Here, we will present preliminary experimental results using Kr to demonstrate their capability of separating ions with a particular charge from those with other charges. The experimental chamber was uniformly filled by Kr sample which was irradiated with a synchrotron radiation in the photoionization region lying between the repeller and extractor electrodes. A pulsed voltage of +75V was applied to the repeller electrode for pushing out photoions, while continuous voltages of 68 and 0 V were applied to the extractor electrode and drift tube , respectively.

Figure 1(a) shows the TOF mass spectra of Kr^{z+} measured in the vicinity of the $3d^1_{5/2}5p^1$ resonance peak at $h\nu$ = 91.2 eV, with the mass gate and retarding electrode being grounded. In order to realize isolation of one of the charged state z from the others, e.g. selecting Kr^{2+} from Kr^{z+} (z = 1-3), the following method was adopted: First, setting the voltage of the mass gate (V_M) to zero, the critical voltage on the retarding grid (V_G) was optimized in such a way that no signal was observed. Now, all the ionic species were reflected back as demonstrated in the Fig. 3 of [1]. Then, a pulsed voltage was applied as V_M, at the timing when a bunch of Kr^{2+} ions arrives at the mass gate, so that they gain additional kinetic energies to overcome the potential barrier at retarding grid and can reach the detector. Figure 1(b) shows the spectrum observed at the same voltage combination as that used in Fig. 1(a) except that V_M and V_G were set to 5 and 75 V, respectively. The width of the V_M was 5 µs and its rising edge was preceded by 22 µs by that of the pulsed voltage applied to the repeller. Only a single peak assigned to Kr^{2+} appears in Fig. 1(b). This confirms that the ion selection using the mass gate works well. We also tested our spectrometer for its capability of separating a specific fragment from the other ions produced from SF_6 (not shown here). From the above observation we consider that this setup can be applied for exclusive imaging detection of C_{58}^{+} after excluding C_{60}^{+} and C_{56}^{+} with the same kinetic energies.
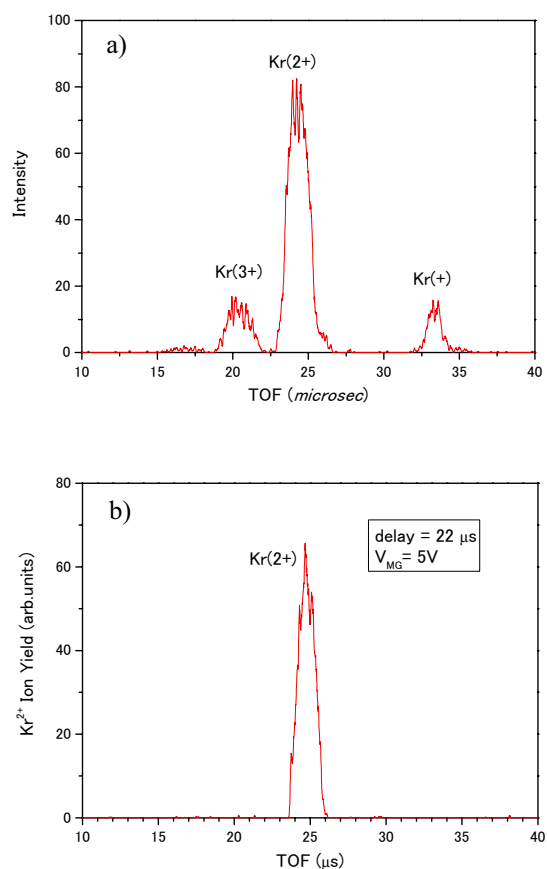

Fig. 1. (a) TOF spectrum of Kr at $h\nu$ = 91.2 eV. The mass gate and retarding grid are kept grounded. (b) TOF spectrum of Kr measured with V_M = 5 V and V_G = 75 V.

[1] B. P. Kafle, H. Katayanagi and K. Mitsuke, AIP Conf. Proc. **879** (2007) 1809.
[2] Md. S. I. Prodhan *et al.*, Chem. Phys. Lett. **469** (2009) 19.
[3] H. Katayanagi *et al.*, in preparation.

Ⅲ-3. MOLECULAR SPECTROSCOPY AND DYNAMICS

Ion Imaging Study of Dissociative Photoionization of C_{60}

H. Katayanagi[1, 2], C. Huang[1], S. I. Prodhan[2], H. Yagi[1], B. P. Kafle[2],
K. Nakajima[3] and K. Mitsuke[1, 2]

[1]*Department of Photo-Molecular Science, Institute for Molecular Science, Okazaki 444-8585, Japan*

[2]*Graduate University for Advanced Studies, Okazaki 444-8585, Japan*

[3]*Science Research Center, Hosei University, Tokyo 102-8160, Japan*

The photoion images of fullerene molecular beams, which consist of parent and fragment ions, were obtained by the velocity map imaging (VMI) technique [1]. The fragments were observed as weak shoulders in transverse profiles of the beam.

The design of our imaging setup was described elsewhere [2, 3]; we explain the experimental procedure briefly. The fullerene (C_{60}) sample was loaded in a cylindrical quartz cell and heated up by a heater around 700-800 K in vacuum. The C_{60} vapor passed through two apertures and reached the ionization region, where the C_{60} molecular beam intersected the monochromatized synchrotron radiation (SR). Ions produced at the ionization region were extracted by a VMI electrode assembly and projected on to a position sensitive detector (PSD) of 40 mm in diameter and 375 mm away from the ionization region. No mass selection was made. We thus obtained two-dimensional projections of three-dimensional scattering distributions of the ions on the PSD.

The photoion images were recorded in the photon energy range from 60 to 110 eV. Fig. 1 shows the photoion images at 60 (a) and 110 (b) eV. Vertical stripes along x axis correspond to the beam. Images of other photon energies resemble the images shown here. Background images obtained without the C_{60} beam was subtracted from all the images.

Figure 2 shows one-dimensional projections of the images along y axis with integration of pixel intensities with respect to x. These projections can, therefore, be regarded as the transverse intensity profiles of the beam. An intense central component of the profiles originates from parent ions of C_{60}. In addition to the intense component, we can recognize shoulders on both sides. Intensities and widths of the shoulders increased with increasing photon energy. The shoulders can be assigned to the photofragments produced by the dissociative photoionization of C_{60} with SR, since the fragments obtained translational energy by the dissociative photoionization and escaped from the central component. This assignment is supported by computer simulations of C_{60} fragmentation. The shapes of the shoulders agreed qualitatively with results of the simulations. Furthermore, the energy dependence can be interpreted as that the smaller and more highly translationally accelerated fragments can be produced with increasing photon energy. This interpretation agrees with our previous conclusions on the

dissociation dynamics of fullerenes [4, 5].

In the present study, we found that the fragments could be observed even without mass selection. The mass selection will allow us more quantitative analyses on translational energy release distributions. We developed a potential switch mass gate [2], which enables us to select a specific fragment from a series of fragments. We are now testing the mass gate experimentally.
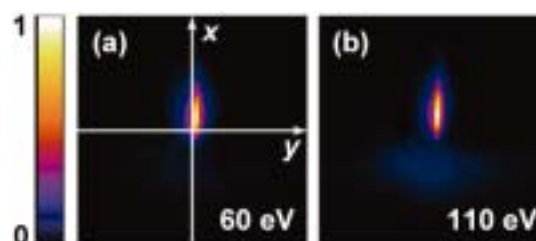

Fig. 1. Photoion images of C_{60} molecular beams (parent and fragment ions) at 60 (a) and 110 (b) eV. In panel (a), x axis corresponds to the direction of the molecular beam and y axis to the synchrotron radiation. Images are 22.5×22.5 mm in size. Pixel size is 0.176×0.176 mm.
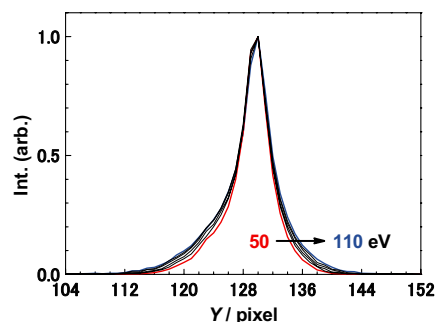

Fig. 2. Transverse intensity profiles of the beam. Curves are plotted every 10 eV in the photon energy range from 50 to 110 eV. Peak intensities of the curves are normalized to unity.

[1] A. T. J. B. Eppink and D. H. Parker, Rev. Sci Instrum. **68** (1997) 3477.

[2] B. P. Kafle *et al.*, AIP Conf. Proc. **879** (2007) 1809.

[3] S. I. Prodhan *et al.*, Chem. Phys. Lett. **469** (2009) 19.

[4] J. Kou *et al.*, Phys. Chem. Chem. Phys. **7** (2005) 119.

[5] K. Mitsuke *et al.*, AIP Conf. Proc. **811** (2006) 161.

Ⅲ-3. MOLECULAR SPECTROSCOPY AND DYNAMICS

Dissociative Photoionization of Perfluorocyclobutane

K. Okada[1, 2], M. Sakai[1], C. Huang[2], H. Yagi[2], H. Katayanagi[2, 3],
K. Mitsuke[2, 3] and K. Tabayashi[1]

[1]*Department of Chemistry, Hiroshima University, Higashi-Hiroshima 739-8526, Japan*
[2]*Institute for Molecular Science, Okazaki 444-8585, Japan*
[3]*Graduate University for Advanced Studies, Okazaki 444-8585, Japan*

Molecular photoionization and ionic fragmentation processes are of fundamental importance in the upper-atmospheric chemistry and plasma physics. Perfluorocyclobutane is extensively used as a reagent for dry etching of semiconductors. Ravishankara *et al.* [1] report that the lifetime of this molecule in the atmosphere is about 1000 years. The use of the gas in industry has atmospheric implications for global warming. Because of the absence of data above the excitation energy of 27 eV, we measured in this study yield spectra of the fragment ions produced by the photoionization of perfluorocyclobutane.

The experiments have been performed on the beamline BL2B at the UVSOR facility. The experimental setup has been described in a previous paper [2], except a minor change for the purpose in this study: A thickness monitor was removed and a needle for gas inlet was installed. Synchrotron radiation was irradiated at right angles to the effusive beam of the sample gas. Fragment ions produced in the ionization region were extracted by a pulsed electric field toward a time-of-flight (TOF) spectrometer. The pulse and ion signals were fed into the start and stop pulse inputs of a multi-stop time-to-digital converter (FAST ComTec, model P7888), respectively, to record TOF signals. Partial ion yield spectra were obtained by measuring a series of TOF spectra while scanning the photon energy. The pressure in the chamber during the measurements was kept at 1.5×10^{-6} Torr.

A variety of fragment ions such as CF_k^+ ($k = 1–3$), $C_2F_m^+$ ($m = 1–4$), $C_3F_n^+$ ($n = 1–5$), and $C_4F_7^+$ were detected in the TOF spectra. This is in contrast to the previous report [3], in which $C_4F_7^+$ could not be detected by the measurement of threshold photoelectron–photoion coincidence spectra acquired at photon energies of 10–27 eV. However, the production of the $C_4F_7^+$ ion is reasonable as observed in this study, if considering the fragmentation of other perfluorocarbon compounds.

Figure 1 shows partial ion yield curves of the fragment ions. The branching fractions at the photon energy of 30 eV are 46.2 % ($C_3F_5^+$), 37.5 % ($C_2F_4^+$), 7.2 % (CF_3^+), 3.0 % (CF^+), 1.7 % (CF_2^+), 1.7 % ($C_3F_3^+$), 1.1 % ($C_4F_7^+$) and others. While the $C_3F_5^+$ and $C_2F_4^+$ fragments are most abundant at all the energies studied here, the yield of these ions decreased greatly with increase in the photon energy. The yield at $\sim$ 170 eV becomes about 1/5 of that at 25 eV. The yield of CF_3^+ gives an approximately

constant value up to 55 eV, and decreases monotonically at the higher energies. The yield of CF^+ increases with the photon energy up to about 80 eV, and then gradually decreases. As a result, the yields of small fragment ions are relatively enhanced with the excitation energy.
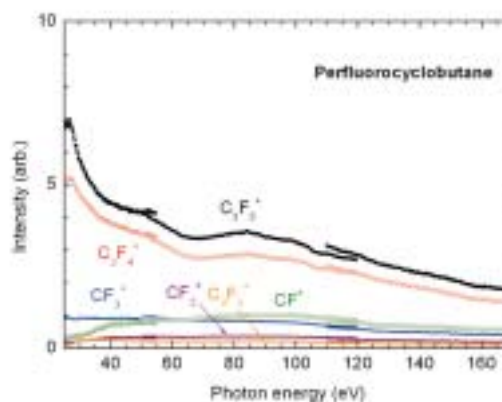

Fig. 1. Partial ion yield curves of the fragment ions produced by the photoionization of perfluoro-cyclobutane.

[1] A. R. Ravishankara, S. Solomon, A. A. Turnipseed and R. F. Warren, Science **259** (1993) 194.
[2] T. Mori, J. Kou, M. Ono, Y. Haruyama, Y. Kubozono and K. Mitsuke, Rev. Sci. Instrum. **74** (2003) 3769.
[3] G. K. Jarvis, K. J. Boyle, C. A. Mayhew and R. P. Tuckett, J. Phys. Chem. A **102** (1998) 3230.

Ⅲ-3. MOLECULAR SPECTROSCOPY AND DYNAMICS

Construction of a Velocity Map Imaging Spectrometer and Its Performance Test Using Rare Gases

Md. S. I. Prodhan[1, 2], H. Katayanagi[1, 2], C. Huang[2], H. Yagi[2],
B. P. Kafle[2], K. Nakajima[2, 3], K. Mitsuke[1, 2]

[1]*The Graduate University for Advanced Studies (SOKENDAI), Okazaki 444-8585, Japan*
[2]*The Institute for Molecular Science, Okazaki 444-8585, Japan;*
[3] *Science Research Center, Hosei University, Tokyo 102-8160, Japan.*

Report is made on velocity map imaging (VMI) spectrometer based on a time-of-flight (TOF) technique. Thus we observed the momentum distributions of the scattered cations produced by dissociative photo-ionization of gaseous fullerenes by irradiation of synchrotron radiation [1, 2, 3]. The basic performance of the spectrometer was tested with rare gases for attaining high kinetic energy resolution of the photofragment images at $h\nu$ = 35 eV and 300 K. The 3D velocity distributions were reconstructed using the inverse Abel transformation (IAT) from the measured 2D images projected on a position-sensitive detector (PSD) to the cross-sectional images in the perpendicular plane of the spectrometer. Using the speed distributions extracted from these cross-sectional images, we evaluated the temperatures by the least-squares fit of the experimental data points to the Maxwell-Boltzmann distributions, as demonstrated in Fig. 1.

In addition, we have reproduced the images of rare gases at 300 K by computer simulations to compare them with those obtained experimentally. The number of He atoms in this simulation was set to 10^5. It was assumed that each He^+ ion flies from the origin with keeping its original thermal velocity of a parent He. The speed was calculated by generating random numbers utilizing Metropolis method from the Maxwell-Boltzmann distribution. The 2D image projected on the PSD was estimated by the spatial density function.

Figure 1 (a) shows the best focused 2D raw image of He^+ ions. The applied voltages at the MCP and electrodes were V_{MCP} = -2200 V, V_R = 640 V, V_T = - 350 V, and V_E = 353 V. Panel (b) represents the cross-sectional image obtained using IAT from Panel (a) [4]. The solid curve in Panel (c) denotes the Maxwell-Boltzmann distribution fitted to the data points (filled circles, extracted from (b)). The temperature obtained by the fittings was 282 ± 2 K which is explained in terms of systematic underestimate inherent in the IAT analysis. Similarly, the temperature was evaluated to be 287 ± 3 K from the simulated image of He^+ in Panel (d). A few scattered data points result from the application of IAT in the image processing.

Similar experimental works were executed for other rare gases, Ne and Ar. All the temperatures were found to be in good agreements with those from the corresponding simulated images.
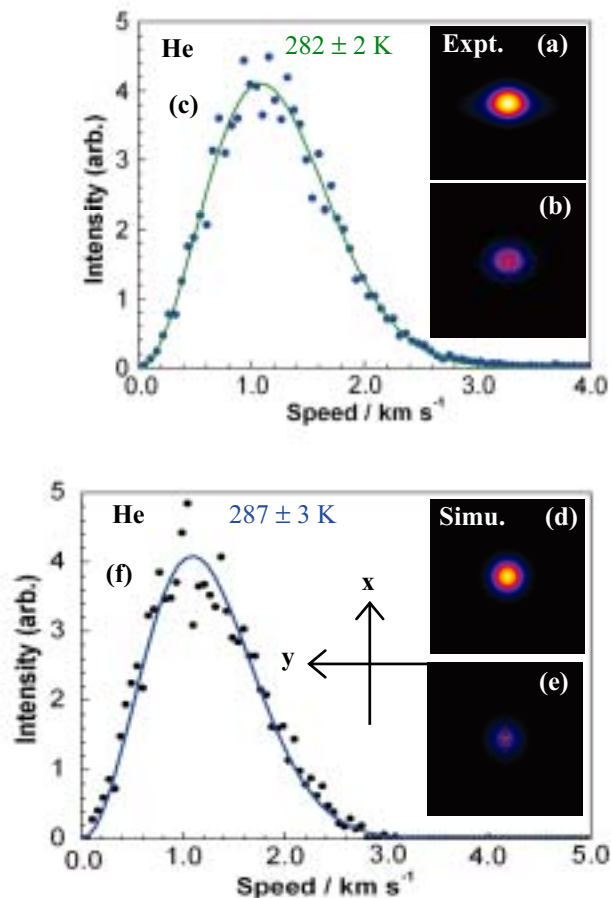

Fig. 1. Panels (a) and (d) show experimental and simulated 2D projections of He^+ ions at 300 K, respectively. Panels (b) and (e) are cross-sectional images obtained from Panels (a) and (d), respectively. Panels (c) and (f) are the speed distributions extracted from Panels (b) and (e), respectively. The solid curves denote the best fitted Maxwell-Boltzmann distributions.

[1] A. T. J. B. Eppink and D.H. Parker, Rev. Sci. Instrum. **68** (1997) 3477.
[2] B. P. Kafle, H. Katayanagi and K. Mitsuke, in "Synchrotron Radiation Instrumentation", Am. Inst. Phys., **CP879** (2007) 1809.
[3] H. Katayanagi *et al.*, Rev. Sci. Instrum. (2008) submitted.
[4] S. M. Candel, Comput. Phys. Commun. **23** (1981) 343.

Exchange Interaction of the Rydberg Electron Bound by Singly Charged Ions in Small Krypton Clusters Studied by X-Ray Absorption Spectroscopy

M. Nagasaka[1], T. Hatsui[2] and N. Kosugi[1]

[1]*Institute for Molecular Science, Myodaiji, Okazaki 444-8585, Japan*
[2]*XFEL Project Head Office, RIKEN, Sayo-cho, Hyogo 679-5148, Japan*

Small krypton clusters show different surface sites (corner, edge, and face), and show different redshifts in the core level as a function of the number of nearest neighbor atoms in X-ray photoelectron spectroscopy (XPS) [1]. The single core hole state formed as a result of core ionization is stabilized by induced polarization (PL) of surrounding atoms, which leads to redshift of the cluster peaks. On the other hand, the excitation to low lying Rydberg states show blueshift of the cluster peaks in X-ray absorption spectroscopy (XAS) [2]. The blueshift behavior indicates destabilization of the excited states, which consist of the Rydberg electron bound by the singly ionized core stabilized by PL. The destabilization would be introduced by exchange interaction (EX) based on Pauli's exclusion principle for the Rydberg electron overlapping with neighbor atoms. In the present work, we have measured XAS of krypton clusters with $<N>$ ~15, and discuss EX of the Rydberg electron in singly charged ion at different surface sites of krypton clusters [3].

The experiments were performed at BL3U. Krypton clusters were formed by the supersonic gas expansion method. XAS spectra were measured with a time-of-flight mass spectrometer to select only Kr_2^+ dimer ions.

Figure 1 shows XAS spectra of krypton clusters. The $3d_{5/2}^{-1}5p$ Rydberg states of some surface sites are blueshifted from the atomic one, whereas the $3d_{5/2}^{-1}6p$ states are redshifted. The initial state effect in van der Waals clusters is negligible; therefore, the energy shift (ΔE_i) of the Rydberg state ($i = 5, 6$) in XAS is simply given by ΔE_i (XAS) = PL (+1) + EX_i (+1), where PL (+1) is obtained by XPS and is not dependent on each Rydberg state i. Table 1 shows the surface site dependent EX energies of different Rydberg states. EX is found to be almost proportional to the coordination number of nearest neighbor atoms. It means EX is mainly caused by the overlap of the Rydberg electron with the nearest neighbor atoms. EX in the low lying 5p Rydberg electron is larger than the PL effect, whereas EX in the 6p Rydberg electron is smaller than PL. Therefore, the energy shift of the 5p Rydberg state in XAS is blueshifted compared to the atomic one. This is reasonable considering the radius of the 5p Rydberg orbital (3.64 Å) is close to the van der Waals distance of krypton (4.03 Å); on the other hand, the 6p orbital (8.13 Å) is distributed beyond the first coordination shell.

In conclusion, we have measured EX of the Rydberg electron bound by singly charged ion at different surface sites of krypton clusters, and found EX is derived from the repulsive and short-range interaction between the Rydberg electron and the nearest neighbor atoms of the ionized atom. EX is a key to understand the surrounding structure of surface sites in clusters.
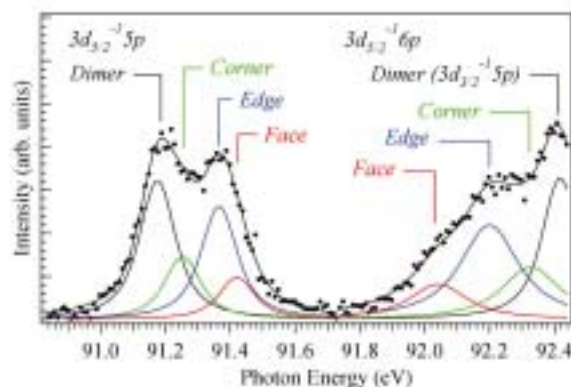

Fig. 1. XAS spectra of different surface sites in krypton clusters with the $3d_{5/2}^{-1}5p$ and $3d_{5/2}^{-1}6p$ states.

Table 1. Exchange (EX) energies (in eV) of Rydberg states at different surface sites of krypton clusters, together with the energy shift (ΔE) in XAS and the induced polarization (PL) energy determined by XPS. The bulk site corresponds to the large clusters [4].

eV	ΔE	PL(+1)	EX (+1)		CN
$3d_{5/2}^{-1}5p$					
Corner	0.05	-0.39	0.44	3.6	3
Edge	0.17	-0.57	0.74	6.0	5
Face	0.22	-0.79	1.01	8.2	8
Bulk	0.40	-1.07	1.47	12	12
$3d_{5/2}^{-1}6p$					
Corner	-0.22	-0.39	0.17	4.9	3
Edge	-0.35	-0.57	0.22	6.3	5
Face	-0.51	-0.79	0.28	8.0	8
Bulk	-0.65	-1.07	0.42	12	12

[1] T. Hatsui *et al.*, J. Chem. Phys. **123** (2005) 154304.
[2] A. Knop, B. Wassermann and E. Rühl, Phys. Rev. Lett. **80** (1998) 2302.
[3] M. Nagasaka, T. Hatsui and N. Kosugi, J. Electron Spectrosc. Relat. Phenom. **166-167** (2008) 16.
[4] M. Tchaplyguine *et al.*, J. Chem. Phys. **127** (2007) 124314.

Ⅲ-3. MOLECULAR SPECTROSCOPY AND DYNAMICS

Formation of Metastable Fragments around the Cl 2p Ionization Thresholds of HCl

Y. Hikosaka, T. Kaneyasu and E. Shigemasa

UVSOR Facility, Institute for Molecular Science, Okazaki 444-8585, Japan

Formation of metastable fragments has recently been found in the inner-shell region of N_2 [1, 2]. The metastable fragments observed trace the formations of high-Rydberg N_2^+ states which dissociate into N^*+N^+ pairs. The N_2^+ states are produced through resonant Auger decay of inner-shell excited states lying below the inner-shell threshold [1] and of multiply excited states lying above the threshold [2]. The N_2^+ states are populated also in the near-threshold region through photoelectron recapture due to the post-collision interaction [1]. These previous works demonstrate that the observation of metastable fragments enables us to probe the decay dynamics of molecular inner-shell excited states [1] and also to perform detailed spectroscopic studies on the multiply excited states embedded in the inner-shell ionization continuum [2].

In this work, we have investigated metastable formation in the vicinity of the Cl 2p ionization thresholds of HCl [3]. The monochromatized SR light and the target gas beam effusing from a hypodermic needle crossed each other at a right angle. Two microchannel plate (MCP) detectors with an active diameter of 14.5 mm, facing each other across the interaction region, were placed at pseudo-magic angles with respect to the electric vector of the light and at right angles with respect to the gas beam [1]. The acceptance solid angle of each MCP detector was estimated to be 0.18 sr. Two grids (80% transmission each) were mounted in front of each detector, and the grids facing the interaction region were grounded. One of the detectors was dedicated to neutral particle observation and the other to fragment ions: the second grid of the neutral particle detector was held at +50 V while that of the fragment-ion detector was held at +5 V. Both the front plates of the two MCP stacks were held around -2 kV in order to prevent detection of electrons. The neutral particle detector was sensitive to neutral metastable particles with sufficient internal energy ($> \sim9$ eV), as well as both VUV and SX photons.

Figures 1(a) and (b) show a fragment ion and a neutral particle yield spectrum measured in the photon energy range of 203.5 - 211.0 eV. The neutral particle yields are due to the detection of neutral metastable fragments, as well as VUV/SX photons. Here, the metastables of the parent HCl cannot be detected with our experimental geometry in which the neutral particle detector is placed perpendicular to the gas flow. Blow the Cl 2p ionization thresholds, Rydberg structures are seen in both the spectra. An intriguing characteristic of the neutral particle yield

spectrum is the broad peaks around the Cl 2p thresholds, which are completely absent from the ion yield spectrum. A similar enhancement of the neutral particle yield is observed around the N 1s ionization threshold of N_2 [1]. In analogy to the N_2 case, we attribute the enhancements in HCl to the observation of metastable fragments formed via either spectator Auger decay from high-Rydberg states or by photoelectron recapture due to the post-collision interaction. Coincidence detections of neutral particle and ions reveal pair formation of H^*+Cl^{n+} [3]. It is found that efficient H^* formation around the ionization thresholds is related to the high-Rydberg HCl^+ states, which are populated via either spectator resonant Auger decay or photoelectron recapture. In addition, H^* is revealed to be produced by the dissociation of the HCl^{2+} states formed by normal Auger decay of the Cl 2p core-ionized states [3].
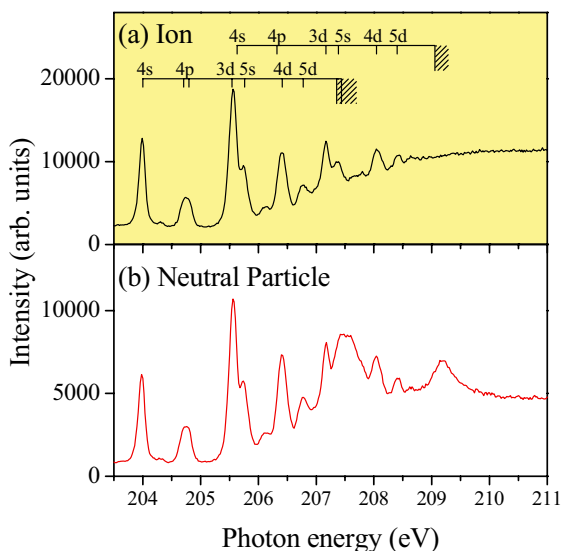

Fig. 1. (a) Ion yields and, (b) neutral particle yields in the vicinity of the Cl 2p ionization thresholds of HCl. The photon energy resolution is set to about 40 meV. The ion yield spectrum was measured with a retardation of +5 V.

[1] Y. Hikosaka, P. Lablanquie and E. Shigemasa, J. Phys. B: At. Mol. Opt. Phys. **38** (2005) 3597.
[2] Y. Hikosaka, T. Gejo, T. Tamura, K. Honma, Y. Tamenori and E. Shigemasa, J. Phys. B: At. Mol. Opt. Phys. **40** (2007) 2091.
[3] Y. Hikosaka, T. Kaneyasu and E. Shigemasa, J. Korean Phys. Soc. **53** (2008) 3798.

High-Resolution Multi-Electron Coincidence Spectrometer for Studies of Atomic and Molecular Auger Processes

Y. Hikosaka and E. Shigemasa

UVSOR Facility, Institute for Molecular Science, Okazaki 444-8585, Japan

When an inner-shell electron in an atom or molecule is removed, the core-hole state decays via the Auger transition. The kinetic energy of the Auger electron is element-specific, and thus Auger electron spectroscopy is widely used as a powerful analytical tool in many different fields of research. However, the detailed interpretation of Auger spectra is difficult, even for atoms and small molecules. This is because inner-shell ionization is concomitant with the excitation and ionization of valence electrons, and all of these core-hole states contribute to the conventional Auger electron spectra. In theory, it is possible to filter out structures due to individual contributions by using the photoelectron-Auger electron coincidence method, which allows one to correlate initial core-hole states with the relevant Auger decays. In practice, the acceptance solid angle of a conventional electron spectrometer is too small to allow the recording of such a coincidence spectrum with sufficient statistics. The experimental limitation was fully solved by the introduction of the magnetic bottle electron spectroscopic technique [1], and highly-efficient coincidence studies using this technique have been successfully performed [2-4]. However, since this technique is based on time-of-flight analysis, the energy resolutions for fast electrons are often insufficient to observe individual Auger lines.

While the retardation of electron kinetic energy improves the energy resolution of time-of-flight analysis in general, the adequateness is not established for the magnetic bottle electron spectroscopic technique using a strong inhomogeneous magnetic field. In this work, we have tested an electric retardation for a magnetic bottle electron analyzer. Our analyzer is essentially the same as that developed by Eland et al. [1], except for the 1.5-m flight path in the present analyzer instead of the original 5-m path. A strong permanent magnet is located close to the interaction region, and the magnetic field guides electrons through a long solenoid toward a position sensitive detector. Electrodes which retard electrons are located around the entrance of the flight tube. The energy resolution was evaluated by measuring He 1s photoelectrons at different photon energies.

Figure 1 shows the evolutions of energy resolution (FWHM) with electron energy, which were observed with a 100-eV retardation or no retardation. It is shown that the retardation improves the energy resolutions. The coincidence measurement of Ar 2p Auger lines demonstrates more clearly the improved

resolution. Figure 2 shows Auger spectra obtained in coincidence with $2p_{3/2}$ photoelectrons; thus, Auger lines associated with the $2p_{1/2}$ core are removed from the ordinary Auger spectrum. While the components of the band structures are not resolved on the spectrum observed without retardation, a 180-eV retardation clearly separates the individual Auger lines.
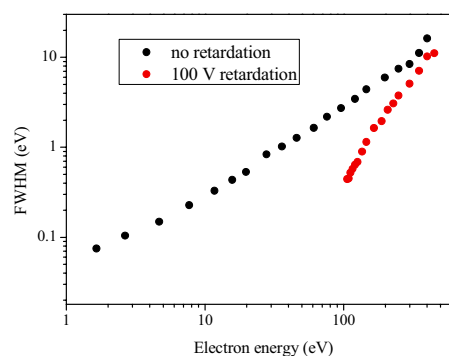

Fig. 1.   Evolutions of energy resolution (FWHM) with electron energy, observed with a 100-eV retardation (red dots) and no retardation (black dots).
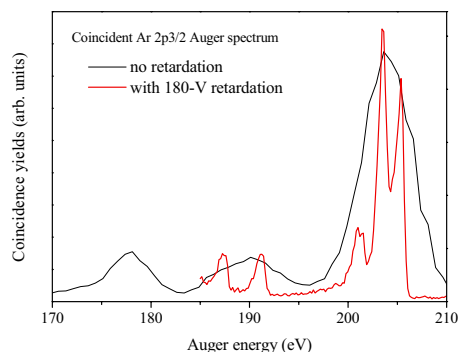

Fig. 2.   Ar 2p Auger spectra obtained in coincidence with $2p_{3/2}$ photoelectrons: with a 180-eV retardation (red) and no retardation (black).

[1] J. H. D. Eland *et al*., Phys. Rev. Lett. **90** (2003) 053003.
[2] Y. Hikosaka *et al*., Phys. Rev. Lett. **97** (2006) 053003.
[3] Y. Hikosaka *et al*., Phys. Rev. Lett. **98** (2007) 183002.
[4] Y. Hikosaka *et al*., Phys. Rev. Lett. **102** (2009) 013002.

Ⅲ-3. MOLECULAR SPECTROSCOPY AND DYNAMICS

Dissociation Pathways of $C_2D_2^{2+}$ Studied by an Auger-Electron–Ion Coincidence Method

E. Shigemasa[1], T. Kaneyasu[1, 2], Y. Hikosaka[1], M. Fushitani[3] and A. Hishikawa[3]

[1]*UVSOR Facility, Institute for Molecular Science, Okazaki 444-8585, Japan*
[2]*Kyushu Synchrotron Light Research Center, Tosu 841-0005, Japan*
[3]*Dept. of Photo-Molecular Science, Institute for Molecular Science, Okazaki 444-8585, Japan*

The acetylene dication is one of the smallest metastable polyatomic dications, whose dissociation and isomarization from the acetylene (HCCH) into the vinylidene (H$_2$CC) configurations have been extensively investigated. By using the PEPIPICO technique, it was found that the acetylene dications dissociate from excited states above 34 eV, where five three-body reactions and three two-body reactions including the dissociation channel via the vinylidene form (CH$_2^+$ + C$^+$: V-channel) have been identified. The isomarization time of the acetylene decation produced following the Auger decay was estimated to proceed within 60 fs [1]. Very lately, the visualization of ultrafast hydrogen migration in deuterated acetylene dication, which occurs in a recurrent manner, was nicely demonstrated by using intense ultrashort laser pulses [2].

An attempt to identify the fragmentation patterns for specific electronic states of the acetylene dication was made more recently, where the momenta of two positively charged ions were measured in coincidence with the Auger electrons [3]. In addition to the V-channel, the other two channels in the two-body reactions, such as the acetylene channel (CH$^+$ + CH$^+$: A-channel) and deprotonation channels (C$_2$H$^+$ + H$^+$: P-channel), were correlated with some Auger final states. In order to gain a further insight into the dissociation mechanism of the Auger final states, we have performed an Auger-electron–ion coincidence study on fragmentations of deuterated acetylene dication, C$_2$D$_2^{2+}$, formed via Auger decay. With the use of our Auger-electron–ion coincidence spectrometer [4], we have identified Auger final states relevant to the individual fragmentations including the three-body reaction, as well as to the formation of metastable C$_2$D$_2^{2+}$.

Figure 1 shows the coincidence Auger spectra extracted from the coincidence data sets, with the maximum intensity in each spectrum normalized to unity. It is found that the atomic fragment ions tend to be produced in the entire region of Auger electrons, while the molecular ions except for CD$^+$ exhibit specific productions for certain Auger final states. The parent dications are mainly observed at the lowest band, which shows a clear maximum around 33.3 eV. The shaded area in the C$_2$D$_2^{2+}$ spectrum displays the CD$^+$ spectrum multiplied by an appropriate factor. We come to the conclusion that the parent dications are essentially produced only from the lowest energy

states with the $1\pi_u^{-2}$ configurations. The second lowest peak in the $1\pi_u^{-2}$ band lies at 34.7 eV, where C$_2$D$^+$ and C$_2^+$ fragments are produced. The CD$_2^+$ fragments related to the V-channel, as well as the atomic fragments C$^+$ and D$^+$ yield the highest energy peak in the $1\pi_u^{-2}$ band at 35.0 eV. The second band around 40 eV in the Auger spectrum seems to be composed of at least three components: 38.5 eV for C$_2$D$^+$ and D$^+$, 40.6 eV for CD$^+$ and D$^+$, and 42.4 eV for C$_2^+$. The highest binding energy band centered at 50 eV enhances violent fragmentation leading to the productions of C$^+$, D$^+$, CD$^+$, and C$_2^+$.
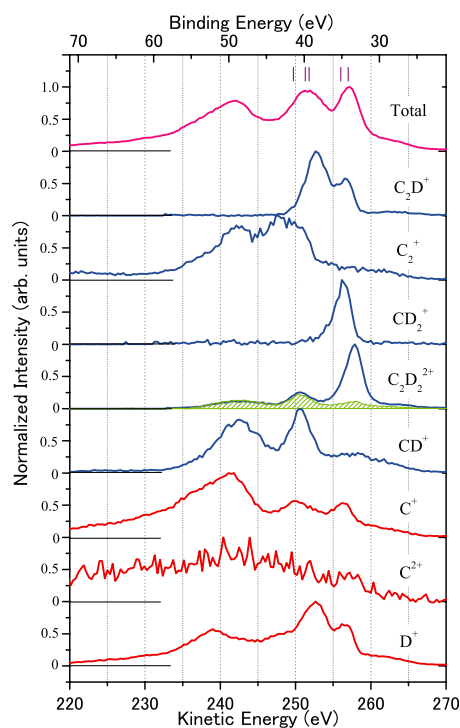

Fig. 1. *KVV* Auger spectrum of C$_2$D$_2$ (pink), in comparison with coincidence Auger spectra related to molecular ions (blue), and atomic ion formation (red).

[1] T. Osipov *et al.*, Phys. Rev. Lett. **90** (2003) 233002.
[2] A. Hishikawa, A. Matsuda, M. Fushitani and E. Takahashi, Phys. Rev. Lett. **99** (2007) 258302.
[3] T. Osipov *et al.*, J. Phys. B **41** (2008) 091001.
[4] T. Kaneyasu, Y. Hikosaka and E. Shigemasa, J. Electron Spectrosc. Relat. Phenom. **156-158** (2007) 279.

Ⅲ-3. MOLECULAR SPECTROSCOPY AND DYNAMICS